Parameterized State Feedback Control applied to the 1st degree of freedom of a cylindric pneumatic robot

Marcos Rijo, Eduardo Perondi, Mário Sobczyk and
Carlos A. C. Sarmanho Jr.

March 11, 2020

Parameterized State Feedback Control applied to the 1st degree of freedom of a cylindric pneumatic robot

Marcos G. Q. Rijo[1], Eduardo A. Perondi[2][0000-0002-6934-7550], Mário. R. Sobczyk[2] S. and Carlos A. C. Sarmanho Jr.[3]

[1]IFSUL Federal Institute, Sapiranga - RS, Brazil
[2] Mechanical Engineering Department, UFRGS University, Porto Alegre - RS, Brazil
[3]IFSUL Federal Institute, Charqueadas - RS, Brazil

Abstract. This paper addresses a gain-schedule trajectory controller applied to the first degree of freedom of a pneumatic five-degree cylindrical robot. The proposed control law is based on pole placement and state feedback techniques associated with a continuous gain-schedule scheme. Its gains are parameterized with respect to the trajectory-dependent mass moment of inertia of the manipulator with relation to its rotation axis. Therefore, the value of the equivalent translational inertia to be moved by the first degree of freedom actuator is calculated on line and used to update the gain set of the controller. As consequence, the poles of the closed-loop system remain unaltered, which results in small performance losses due to payload variations. Performance enhancement is verified by means of experimental results of position trajectory errors for the controlled system considering invariant and variable equivalent mass applied to the 1st DOF.

Keywords: gain-schedule control, state feedback control, pneumatic robotic manipulator.

1   Introduction

Robotic manipulators are driven by electric motors or, less frequently, fluidic ones, according to several performance requirements such as precision, power/weight and power/volume ratios, maintainability, compliance, robustness, durability, reliability, response time, ease to control, energy source availability, energetic efficiency and cost. In this context, pneumatic actuators are attractive because they are fast, low-cost, easy to install (compressed air is common in industrial facilities), and durable, while presenting high power/volume and power/weight ratios. Moreover, air compressibility is useful in collaborative applications since it facilitates handling fragile objects and interacting with humans, thereby enhancing overall compliance. Nevertheless, these actuators are difficult to control accurately for a number of reasons associated with highly nonlinear phenomena such as air compressibility, pressure dynamics in the cylinder chambers, dead zones in the control valves, and dry friction [1]. Thus, significant effort has been spent on improving control algorithms applied to pneumatic actuators, so their considerable operational advantages can be exploited with acceptable accuracy [2].

Due to their highly nonlinear nature, it is widely known that pneumatic actuators are not expected to achieve very good performance in precision applications when controlled by means of common linear feedback strategies, such as PID control [3-5]. On the other hand, nonlinear controllers tend to yield significant performance improvements, but at the cost of greatly increased complexity not only in theoretical terms, but also in the corresponding implementation hardware [6]. Thus, intermediate complexity algorithms such as State Feedback Control with position, velocity and acceleration feedback (the PVA controller) can often be regarded as an interesting "midway" approach, yielding acceptable performance at relatively reduced implementation costs when compared to more advanced algorithms such as Computed Torque Control [6].

When a linear model is provided, PVA control allows imposing the desired closed-loop dynamics to the system (at least for a limited range) with relatively little effort in design and implementation. If applied to pneumatic actuators, such controllers yield good responses when the mass is held constant, but its dynamic performance deteriorates with varying payloads, as demonstrated experimentally in [4]. When translated to the case of a pneumatically driven robot, this results in poor accuracy even if the payload remains constant, because pose variations will also affect the controller performance due to changes in the overall equivalent inertia perceived in each joint.

Here, we improve the PVA-controller robustness with respect to payload variations by parameterizing its gains in terms of the moment of inertia associated with the instantaneous robot pose, an approach that can be interpreted as a continuously updated gain-schedule control algorithm. It is applied to compensate for the variations in the moment of inertia perceived in the 1st degree of freedom (DOF) of a 5-DOF cylindrical robotic manipulator driven by a pneumatic power source. The performance of the proposed controller is evaluated experimentally, using the results obtained with a standard PVA-controller as reference for comparison.

Section 2 of this paper addresses the overall configuration of the pneumatic robot. Section 3 is dedicated to defining the equivalent mass perceived by the actuation system of the 1st DOF as a function of the manipulator pose. The synthesis of the control strategy is presented in Section 4, whereas experimental results are discussed in Section 5. Finally, the main conclusions are presented in Section 6.

2   The 5-DOF Pneumatic Robot

As shown in Fig. 1, the robot comprises one rotation joint related to the 1st DOF, followed by two prismatic orthogonal joints associated to the 2nd and 3rd DOFs, and two rotation joints associated to the 4th and 5th DOFs. The end effector is composed by a pneumatic gripper with two fingers. The first joint is driven by a rodless double action cylinder, connected with a 5/3 proportional valve to control the air mass flow rates that fill or exhaust the actuator chambers. Chamber are measured through pressure transducers. These components are mounted in a base constructed with aluminum profiles. Some of these hollow profiles are also used as accumulators for the compressed air coming from the pneumatic supply line, reducing its pressure oscillations. The robot base also houses a transmission system of three pulleys and a synchronizer belt, which

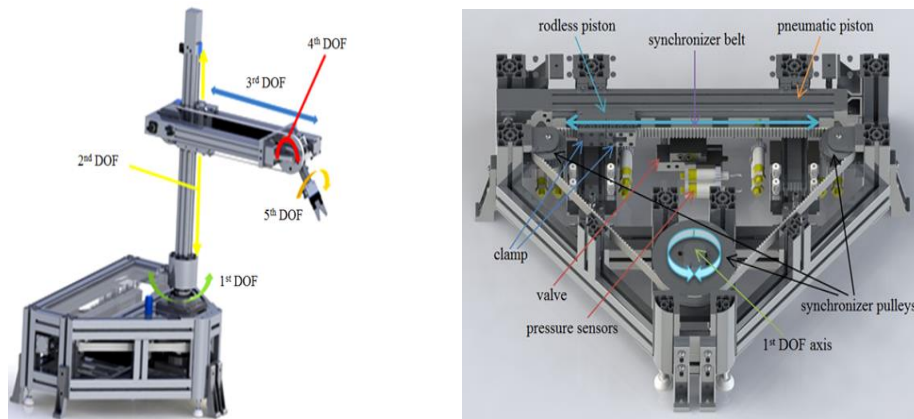convert the piston translation of the piston into the rotational movement of the 1st DOF of the robot.

Fig. 1. Kinematic chain of the pneumatic cylindrical robot (left) and schematic view of the mechanical components of the 1st degree of freedom (right).

The main part of the transmission system of the 1st DOF is a timing belt pulley (primary pulley), assembled to a vertical rotational aluminum shaft that supports all other links of the robot. This pulley is connected to the other two by a timing belt, which ensures that all three rotations are synchronized. A metallic clamp is used to connect the extremities of the timing belt, which transmits the force from the pneumatic actuator to the pulley linked to the 1st joint. The timing belt is of HTD type, which, according to [7], is adequate for low speeds and high torque transfer operations.

A proprietary Microcontrolled Actuation and Control Unit (UCAM) was developed to communicate the control board with the measurement devices. Typical functions of UCAM include analogic signals sampling from pressure sensors, A/D and D/A conversions, and performing the serial communication (RS-485) with the magnetostrictive piston position sensor mounted inside of the pneumatic cylinder. A centralized robot control algorithm is programmed in Matlab-Simulink® and is processed in a PC hosted dSPACE® DS-1104 board with a hard real-time control cycle of 1.8 ms.

3 Parameterization of the equivalent mass

As the robot moves, the moment of inertia with respect to the rotation axis of the 1st DOF changes with the current robot joint coordinate values. The parametric control strategy is based on, by means the Steiner's law, calculate a so-called *equivalent lumped mass* that is instantaneously added to that of the moving parts of its linear pneumatic cylinder, resulting in the value of the total *equivalent* mass that have to be moved by the linear piston in result of the control driving. Taking into account this value, the gains of the state feedback controller are suitably updated by means a parametric algorithm.

Therefore, when the arm changes its pose, the control gains are modified, seeking to keep constant the closed-loop poles associated with the 1st DOF. This strategy takes into account the positions of the 3rd and 4th DOFs of the robot, which alter the mass moment of inertia with respect the 1st DOF. Fig. 2 presents the definition of the coordinate systems.
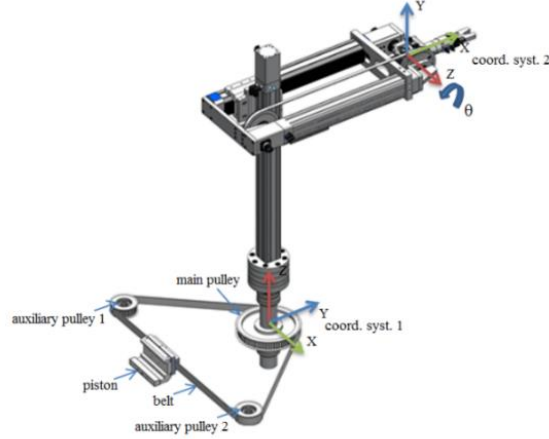

Fig. 2. Manipulator and coordinate systems for the moment of inertia parameterization

The moment of inertia I of a given robot link with respect to the 1st DOF Z-axis is:

$$I = I_G + md^2, \tag{1}$$

where m is the link's mass, I_G is the link mass moment of inertia related to its mass center, and d is the distance from this mass center to the 1st DOF Z-axis.

To parameterize its equivalent lumped mass, the manipulator was divided into three subsets. The first one comprises the transmission shaft and the pulleys of the 1st DOF, the coupling part between the 1st and 2nd DOFs, the pneumatic actuator of the 2nd DOF, the coupling part between the 2nd and 3rd DOFs, and the piston of the 3rd DOF actuator. Since no one of these moving parts affects the mass moment of inertia with respect to the 1st DOF Z-axis, its equivalent lumped mass m_{E1} is constant.

The second subset is formed by the actuators of the 3rd and 4th DOFs. When these parts move, the mass moment of inertia relative to 1st DOF Z-axis varies. Thus, m_{E2} represents the inertia variations due to the displacements in the 3rd DOF, whereas the effects of the 4th DOF are represented by another variable equivalent mass m_{E3}. The equivalent lumped mass for this subsystem is given by $m_{E2} + m_{E3}$.

The third subset is formed by the wrist, whose mass moment of inertia I_G varies with the translation of the 3rd DOF and the rotation θ of the 4th DOF, for that, Steiner's law is used:

$$I_G = \left(\frac{I_{XG}+I_{YG}}{2}\right) - \frac{I_{XG}-I_{YG}}{2}\cos(2\theta) + I_{XYG}\sin(2\theta), \tag{2}$$

where I_{XG}, I_{YG} and I_{XYG} are the wrist moment of inertia relative to the associated axes x, y and the rotation angle θ (Fig. 2). Thus, once obtaining the value of I_G, the equivalent mass m_{E4} is calculated through (1).

After calculating the equivalent masses of the three subsystems, the total equivalent mass is determining by summing all involved masses:

$$m_E = m_{CE} + m_C + 2m_{EP} + m_{E1} + m_{E2} + m_{E3} + m_{E4}, \qquad (3)$$

where m_{CE}, m_C and m_C are, respectively, the piston, clamp and belt masses, whereas $m_{EP} = I_P/R_P^2$ is the equivalent mass of each the auxiliary pulley in the transmission mechanism of the 1st DOF (Fig. 2), with I_P and R_P standing for their mass moment of inertia and effective radius.

4 State feedback controller

The modeling of a standard pneumatic servopositioning system is extensively discussed in several works [3-5, 8], where it is shown to be satisfactorily represented by means of the following transfer function:

$$G(s) = \frac{Y(s)}{I(s)} = \frac{b_0}{s(s^2 + a_1 s + a_2)}, \qquad (4)$$

where I is the control signal voltage applied to the pneumatic servovalve, y is the piston position, s is the Laplace varialble, and b_0, a_1, a_2 are parameters that depend upon the characteristics of the system. These coefficients can be expressed as:

$$b_0 = \frac{4ArRTk_q}{m_E V}; a_1 = \frac{4rA^2 P_0}{m_E V}; a_2 = \frac{C_f}{m_E}, \qquad (5)$$

where A is the cross-sectional area of the pneumatic piston, r is specific heat ratio of the air, R is the gas constant of compressed air, T is the average absolute temperature, V is the volume of the piston, k_q is the average mass flow rate gain of the valve orifices, and C_f is the is the viscous friction coefficient (linear Newton's friction coefficient). Table 1 presents the numerical values used in the present work for the controller design.

Table 1. Numerical values of the model parameters [6].

T	Average absolute temperature [K]	293,15
P_0	Initial pressure in the chambers [Pa]	$3,85.10^5$
R	Gas constant [J/kgK]	286,9
A	Cross-sectional area of the pneumatic piston actuator [m^2]	$8,04.10^{-4}$
r	Specific heat ratio of the air	1,4
k_q	Average mass flow rate gain of the servovalves [kg/s]	$6,7.10^{-3}$
V	Volume capacity of the cylinder [m^3]	$3,62.10^{-4}$
C_f	Viscous friction coefficient [Ns/m]	266,55

6

As the 3rd order model does not present zero-pole cancelation, the system is controllable. Therefore, within the actuating range of its control valve, it is possible to arbitrarily choose its closed-loop poles by using the following feedback law:

$$u(t) = k_p \tilde{y} + k_v \dot{\tilde{y}} + k_a \ddot{\tilde{y}}, \tag{6}$$

where $\tilde{y}$, $\dot{\tilde{y}}$ and $\ddot{\tilde{y}}$ are the errors between the desired values of position (y_d), velocity ($\dot{y}_d$), and acceleration ($\ddot{y}_d$), and their measured counterparts y, $\dot{y}$, and $\ddot{y}$, with respective gains k_p, k_v and k_a. This law is schematically shown in Fig. 3. It is usually referred to as PVA because it uses position (P), velocity (V) and acceleration (A) as feedback states. Several authors applied PVA controllers to pneumatic positioners based on the 3rd order linear model given in (4) [5]. Velocity and acceleration signals were obtained by numerical differentiation of the position data.
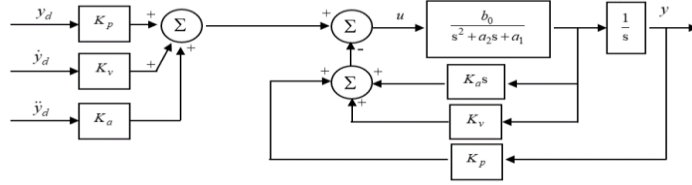

Fig. 3. Linear 3rd order system with state feedback controller.

The characteristic equation for this closed-loop system is

$$s^3 + (b_0 k_a + a_2)s^2 + (b_0 k_v + a_1)s + b_0 k_p = 0. \tag{7}$$

Since each gain affects one independent power of s in Equation (7), the allocation of all three poles is a straightforward process. Defining P_{1d}, P_{2d} and P_{3d} as the desired poles, the correspondent characteristic coefficients are:

$$a_{0d} = -P_{1d} P_{2d} P_{3d}, \tag{8}$$

$$a_{1d} = P_{1d} P_{2d} + P_{2d} P_{3d} + P_{1d} P_{3d}, \tag{9}$$

$$a_{3d} = -(P_{1d} + P_{2d} + P_{3d}). \tag{10}$$

Thus, the desired dynamics' characteristic equation is

$$s^3 + a_{2d} s^2 + a_{1d} s + a_{0d} = 0. \tag{11}$$

Finally, matching equations (7) and (11), the controller gains are determined as:

$$k_p = \frac{a_{0d}}{b_0}; k_v = \frac{a_{1d} - a_1}{b_0}; k_a = \frac{a_{2d} - a_2}{b_0}. \tag{12}$$

The desired dynamics is defined as a dominant pair of poles for the 1st DOF (approaching its dynamics of that of a 2nd order system), with the third pole located in a

position ten times farthest than the real part of the dominant ones. The maximum over-shoot is chosen as 20% and the settling time is 1.4 s (with 2% tolerance), implying a damping $\zeta=0{,}5$ and a natural frequency $\omega_n=5{,}71$ rad/s. The corresponding complex conjugate poles are $P_{12d} = -2{,}86 \pm 4{,}95i$, whereas the third pole is $P_{3d} = -28{,}6$. Once the desired dynamics is established, the complete proposed control strategy consists of performing the following three steps on each control cycle:

1. Compute the equivalent total lumped mass value as described in (3);
2. Update the open loop coefficients (b_0, a_1 and a_2) using (5);
3. Calculate the control gains k_p, k_v and k_a (12) and obtain the corresponding control signal to be applied to the servovalve (6).

5   Experimental Results

Two cases were analyzed through experimental tests. In the first, only the 1st DOF was moved, whereas the 3rd and 4th arm joints were fixed so as to generate three conditions for the equivalent moment of inertia: maximum, medium, and lowest. In the second one, all these three joints were made to track their respective desired trajectories, as described in Table 2, so that the equivalent inertia with respect to the 1st DOF was continuously varying. In both cases, two PVA controllers were used: a *standard* (SPVA) one, based on the nominal values of the linear model for the 1st DOF, and the proposed *parameterized* (PPVA) one, with continuously updated gains.

Table 2. Desired trajectories

$y_{d\_1st}(t)\,[m] =$		$y_{d\_3th}(t)\,[m] =$		
	0,13		0	$t < 10$
	$0{,}57\left(\frac{t-10}{3}\right)^5 - 1{,}425\left(\frac{t-10}{3}\right)^4 + 0{,}95\left(\frac{t-10}{3}\right)^3 + 0{,}13$		$1{,}5\left(\frac{t-10}{3}\right)^5 - 3{,}75\left(\frac{t-10}{3}\right)^4 + 2{,}5\left(\frac{t-10}{3}\right)^3$	$10 \le t < 13$
	0,225		0,25	$13 \le t < 23$
	$0{,}57\left(\frac{t-23}{3}\right)^5 - 1{,}425\left(\frac{t-23}{3}\right)^4 + 0{,}95\left(\frac{t-23}{3}\right)^3 + 0{,}225$		$0{,}3\left(\frac{t-23}{3}\right)^5 - 0{,}75\left(\frac{t-23}{3}\right)^4 + 0{,}5\left(\frac{t-23}{3}\right)^3 + 0{,}25$	$23 \le t < 26$
	0,32		0,3	$26 \le t < 36$
	$-0{,}57\left(\frac{t-36}{3}\right)^5 + 1{,}425\left(\frac{t-36}{3}\right)^4 - 0{,}95\left(\frac{t-36}{3}\right)^3 + 0{,}32$		$-0{,}3\left(\frac{t-36}{3}\right)^5 + 0{,}75\left(\frac{t-36}{3}\right)^4 - 0{,}5\left(\frac{t-36}{3}\right)^3 + 0{,}3$	$36 \le t < 39$
	0,225		0,25	$39 \le t < 49$
	$-0{,}57\left(\frac{t-49}{3}\right)^5 + 1{,}425\left(\frac{t-49}{3}\right)^4 - 0{,}95\left(\frac{t-49}{3}\right)^3 + 0{,}225$		$-1{,}5\left(\frac{t-49}{3}\right)^5 + 3{,}75\left(\frac{t-49}{3}\right)^4 - 2{,}5\left(\frac{t-49}{3}\right)^3 + 0{,}225$	$49 \le t < 52$
	0,13		0	$52 \le t \le 60$
$y_{d\_4th}(t)\,[rad] =$	2,817			$t < 23$
	$-16{,}191\left(\frac{t-23}{3}\right)^5 + 40{,}477\left(\frac{t-23}{3}\right)^4 - 26{,}985\left(\frac{t-23}{3}\right)^3 + 2{,}817$			$23 \le t < 26$
	0,1185			$26 \le t < 36$
	$16{,}191\left(\frac{t-23}{3}\right)^5 - 40{,}477\left(\frac{t-23}{3}\right)^4 + 26{,}985\left(\frac{t-23}{3}\right)^3 + 0{,}1185$			$36 \le t < 39$
	2,817			$39 \le t \le 60$

Due to the geometric configuration, the 2nd (vertical displacement) and the 5th DOF do not significantly influence the mass moment of inertia of the entire manipulator with respect to the 1st DOF. Therefore, only the 3rd and the 4th DOF displacement were taken into account in the variable mass case tests, in which, the desired trajectory consists of a combination of a 7th order polynomial curve with constant values in the initial and final positions, as presented on Table 2. These kinds of trajectory have already been

used as a test pattern in other studies of tracking control [8] and was prescribed in a way that the manufacturer pneumatic cylinder's limits of velocity and acceleration are always observed. Figure 4 presents the desired trajectory for the 1st DOF.

5.1 Case 1 – Invariant equivalent mass applied to the 1st DOF

In this case, the tests were performed with three different geometric configurations of the robot, where the 3rd and 4th DOF were fixed so the equivalent mass perceived in the 1st DOF presented minimum (86.5 kg), intermediate (134 kg) and maximum values (180.5 kg). For simplicity, the results shown in this section refer only to the minimum inertia case. The trajectory-tracking errors in all cases are discussed in Section 5.3.

A typical trajectory tracking position for both controllers when the system operates with the minimum inertia is presented in Figure 4.

(a) PPVA (b) SPVA
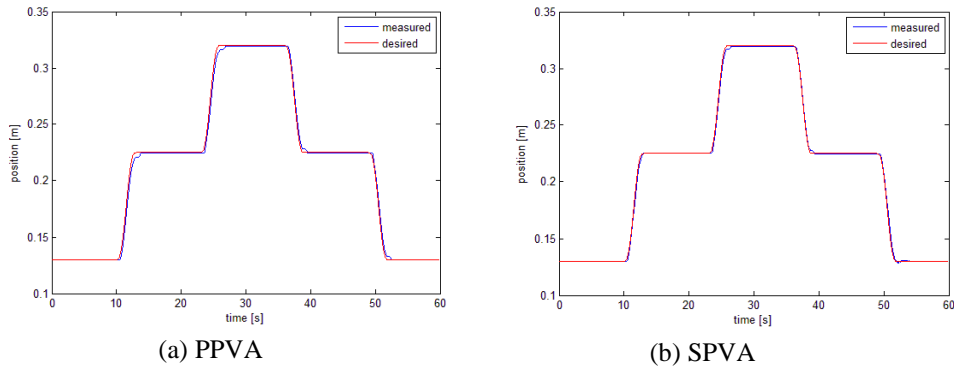
Fig. 4. Position trajectory tracking response (smaller inertia case: 86,5 kg).

Figure 5 presents the control signals for the minimum inertia case.

(a) PPVA (b) SPVA
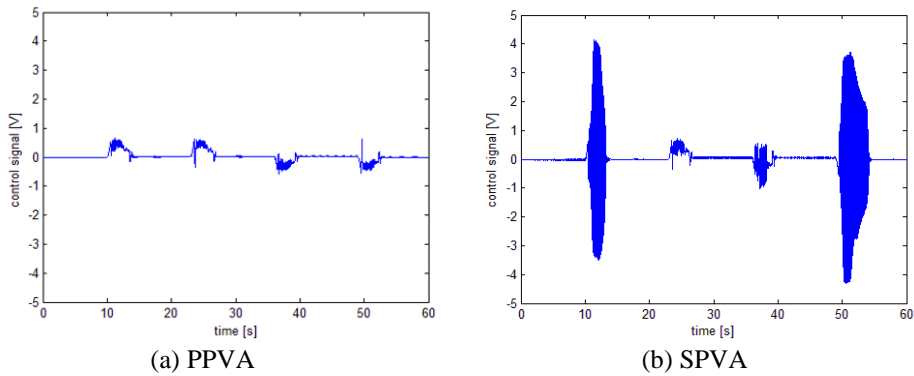
Fig. 5. Control signals for minimum inertia case.

It is clear that the control action required for the SPVA control law is much more severe than the one given in the PPVA case. Although no saturation occurred (the valve operates in the range of -5 V to +5 V), the chattering in control action for the PPVA is undesirable because it leads to premature wear of the control valve and to the risk of exciting unmodeled dynamics in the robot arm. In fact, when this law was used, it was possible to observe vibrations along the arm structure.

5.2 Case 2 – Variable equivalent mass applied to the 1st DOF

Aiming at reproducing actual operation conditions, each DOF tracks its respective desired trajectory as defined in Table 2, so the equivalent mass with respect to the 1st DOF is time-varying, as depicted in Figure 6.
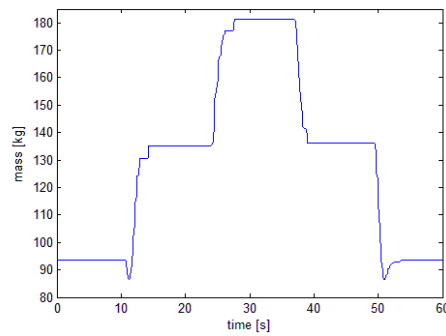
Fig. 6. Time evolution of the equivalent mass calculated through (4).

Figure 7 present the position tracking and position tracking error for the two control algorithms operating with all the joints moving concomitantly.

| (a) PPVA | (b) SPVA |
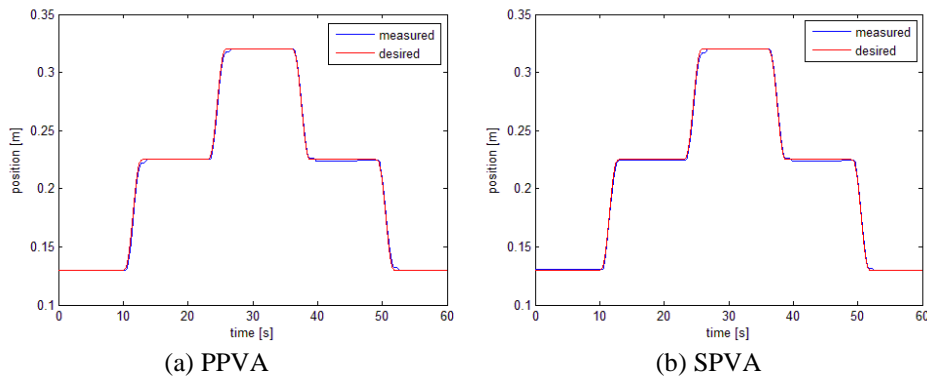
Fig. 7. Position trajectory tracking response (variable inertia).

Figure 8 shows the control actions applied to the valve for both controllers.
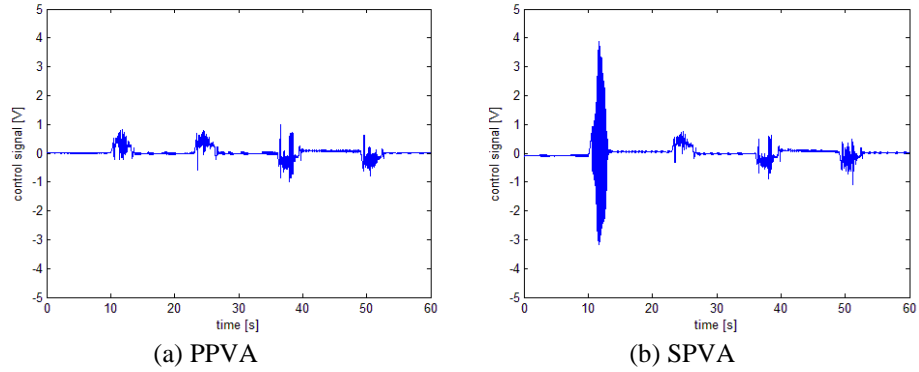
(a) PPVA   (b) SPVA

Fig. 8. Control signals for the time varying inertia case.

Once again, it is clear that the use of the proposed PPVA scheme leads to reductions in the chattering of the valve opening, which is desirable.

5.3 Position trajectory-tracking errors

The results plotted in Fig. 9 presents the position trajectory-tracking errors in the closed-loop system for all performed tests. These results are also summarized numerically in Table 3.
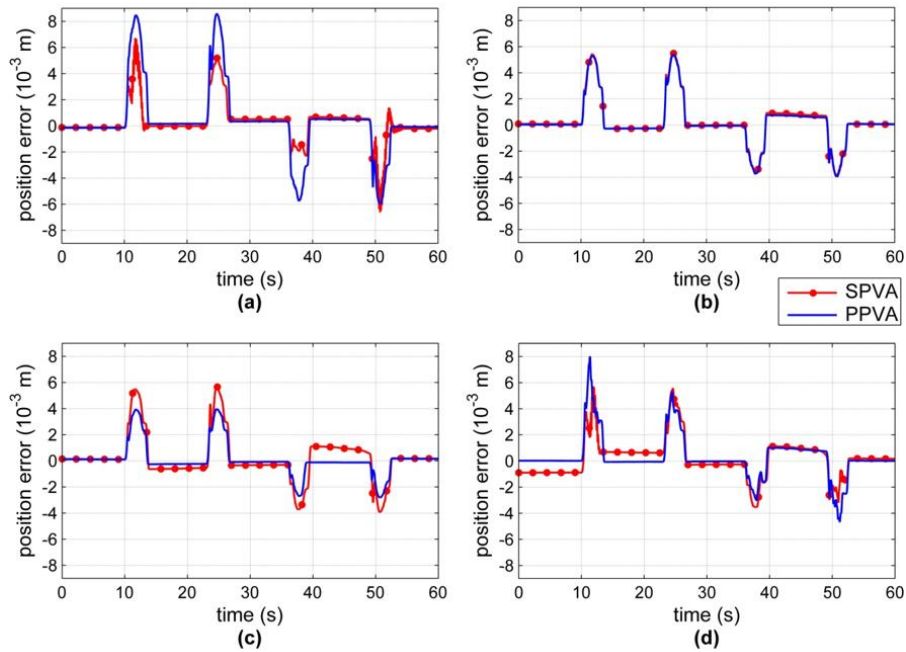

Fig.9. Trajectory-tracking errors for the controlled system: (a) minimum mass, (b) nominal mass, (c) maximum mass, (d) time-varying mass.

Table 3. Table 4. Experimental results summary

Mass [kg]		Steady State Error [mm]		Tracking error [mm]		
		Max.	Average	Max.	Average	Gains
Variable	🟦	0,73	0,21	7,95	5,25	Parameterized
	🟥	0,63	0,38	5,72	4,52	Fixed
86,5	🟦	0,47	0,26	8,58	7,20	Parameterized
	🟥	0,53	0,32	6,72	5,23	Fixed
134	🟦	0,57	0,24	5,42	4,61	Parameterized
	🟥	0,69	0,26	5,52	4,63	Fixed
180,5	🟦	0,24	0,15	3,98	3,37	Parameterized
	🟥	0,57	0,40	5,72	4,73	Fixed

Overall, error amplitudes are similar for both controllers, suggesting no clear advantage for the proposed scheme. However, closer inspection shows that PPVA control leads to significant reductions in steady-state errors, especially when the inertia in the actual system is larger than the estimate used in designing the SPVA. Coupled with the chattering reduction observed in the previous sections, this indicates that the proposed controller tends to improve the precision of the robot arm as a whole, since it reduces steady-state errors *and* structure vibrations as the overall trajectory is performed.

Still with respect to steady-state errors, this result is in apparent contradiction with the corresponding open-loop linear system model given in (4): since there is a pole on the origin, the corresponding integral action should force these errors to zero. However, we must stress that the *real* system is highly nonlinear, with at least two major hindrances to such "ideal" integral action: (i) dry-friction forces, which cause the actuating piston to stick unless pneumatic forces are high enough to cause movement [10]; (ii) a dead zone in the control valve, which, for the employed model, is typically about 5% of its opening stroke. Thus, small but nonzero steady-state errors are to be expected when PVA-control is applied to this type of system.

6   Conclusions

Even though there is no significant reduction in error amplitudes when compared to a standard, fixed-gain PVA controller, the proposed parameterized control scheme leads to important reductions in the steady state error values, especially when the real inertia in the system is greater than expected during the design of the standard controller. Moreover, the proposed algorithm leads to significantly reduced chattering in the corresponding control signals applied to the servovalve. This particular result is highly desirable, since it leads to extended lifespan of the control valves and reduced vibrations in the overall structure of the robotic arm. For these reasons, the proposed control scheme can be considered an attractive one.

Further work would include stability and robustness analysis of the proposed parameterized PVA control scheme, as well as the extension of this technique to compensate for other undesirable effects in the system.

12

References

1. Saravanakumar D, Mohan B, Muthuramalingam T (2017) A review on recent research trends in servo pneumatic positioning systems. Precision Engineering, July 2017, Vol.49, pp.481-492, DOI:10.1016/j.precisioneng.2017.01.014.
2. Rouzbeh B; Bone GM ; Ashby G (2018) High-accuracy position control of a rotary pneumatic actuator. Mechatronics, IEEE/ASME Transactions on, December 2018, Vol.23(6), pp.2774-2781, DOI: 10.1109/TMECH.2018.2870177.
3. Bobrow J E, McDonell B W (1998), Modeling, identification, and control of a pneumatically actuated, force controllable robot. IEEE Transactions on Robotics and Automation, October 1998, Vol.14(5), pp. 732-742.
4. Ning S, Bone GM (2002) High steady-state accuracy pneumatic servo positioning system with PVA/PV control and friction compensation, Proceedings of the 2002 IEEE International Conference on Robotics and Automation, Washington, DC, pp. 2824-2829.
5. Sobczyk MR, Perondi EA, Suzuki R (2012) Feedback linearization control with friction compensation applied to a pneumatic positioning. ABCM Symposium Series in Mechatronics - Vol. 5 2012. Section II – Control Systems, pp 252-261.
6. Sarmanho CAC Jr (2014), Desenvolvimento de um robô pneumático de 5 graus de Liberdade com controlador não linear com compensação de atrito. Thesis (PhD in Mechanical Engineering), Universidade Federal do Rio Grande do Sul.
7. Urethane Timing Belts and Pulleys GATES CATALOG. www.http://misbelt.com/wp-content/uploads/2018/01/Mectrol-Belt-Pulley-Catalog_5_11.pdf.
8. Virvalo, T. (1989) Designing a Pneumatic Position Servo System. Power International, v.35, pp.141-147.
9. Borges FAP, Perondi EA, Sobczyk MR., Cunha MAB (2019), A hydraulic actuator model using feedforward neural networks, 25th ABCM International Congress of Mechanical Engineering - October 20-25, 2019, Uberlândia, MG, Brazil.
10. Sobczyk M R, Gervini VI, Perondi E A, Cunha, M A B (2016) A continuous version of the LuGre friction model applied to the adaptive control of a pneumatic servo system. Journal of the Franklin Institute,Vol.353(13), pp. 3021-3039.